

Regime diagrams and characteristics of flame patterns in radial microchannels with temperature gradients

Aiwu Fan^{a,b,*}, Sergey Minaev^c, Sudarshan Kumar^d, Wei Liu^b,
Kaoru Maruta^a

^a Institute of Fluid Science, Tohoku University, 2-1-1 Katahira, Aoba-ku, Sendai, Japan

^b School of Energy and Power Engineering, Huazhong University of Science and Technology, Wuhan, China

^c Institute of Theoretical and Applied Mechanics, SB-RAS Novosibirsk, Russia

^d Aerospace Engineering Department, IIT Bombay, Powai, Mumbai, India

Received 15 June 2007; received in revised form 2 October 2007; accepted 16 October 2007

Available online 21 December 2007

Abstract

Comprehensive regime diagrams of flame pattern formation in radial microchannels with temperature gradients were drawn based on experimental findings. A premixed methane–air mixture was introduced at the center of microchannels formed by two parallel circular quartz plates that were heated with an external porous burner to create a positive temperature gradient condition in the direction of flow. Combustion behavior in those microchannels at channel widths of 0.5, 1.0, 1.5, 2.0, 2.5, and 3.0 mm were experimentally investigated. Regime diagrams of various stable and unstable flame patterns were obtained, confirming that the flame pattern is a strong function of mixture equivalence ratio, inlet mixture velocity, and channel width. Furthermore, some combustion characteristics, such as the rotating frequency of the single pelton-like flame and the triple flame, the radius of the stable circular flame front, and comparison between the major combustion products of the single and double pelton-like flames, were also investigated.

© 2007 The Combustion Institute. Published by Elsevier Inc. All rights reserved.

Keywords: Microscale combustion; Flame pattern; Rotating frequency; Flame radius; Combustion products

1. Introduction

In combustion at normal scales, the phenomena of pattern formation and flame front instabilities have been extensively investigated. For instance, cellular flames [1,2], kink flames [2], rotating spiral flames

[3–6], target flames [6], and triple flames [7] have been widely observed in gaseous premixed and non-premixed combustion systems. Different types of flame instability, such as hydrodynamic, buoyancy-driven, thermal-diffusive, and viscous fingering, have been reported in the literature [8–11]. These phenomena are quite complex, as the process is governed by the coupling of fluid dynamics, chemical reaction, and heat and mass transfer properties of fuel and oxidizer.

Recently, microscale combustion has been attracting increasing attention [12–34] due to its major advantages. These advantages include energy densities

* Corresponding author at: Institute of Fluid Science, Tohoku University, 2-1-1 Katahira, Aoba-ku, Sendai, Japan. Fax: +81 22 217 5220.

E-mail address: faw@edyn.ifs.tohoku.ac.jp (A. Fan).

Nomenclature

| | | | |
|---------------------|---|------------------|--|
| b | Channel width (mm) | T_{top} | Wall temperature at the inner surface of the top plate (K) |
| r | Radial location in the microchannel (mm) | V_{in} | Inlet velocity in the mixture delivery tube (m/s) |
| T_{bottom} | Wall temperature at the inner surface of the bottom plate (K) | ϕ | Equivalence ratio |
| | | \varnothing | Diameter (mm) |

of hydrocarbon fuels that are higher than those of electrochemical batteries (~ 20 – 50 times higher) and abatement of pollutant emission due to lower operating temperatures [15,20]. However, the increased heat loss due to large surface area–volume ratios adversely affects the combustion stability limits in devices and systems employing microscale combustion as well as wall radical destruction does. For stable combustion, thermal management, for instance, heat recirculation, is a key factor for efficient operation of these microscale combustion devices [16,17,20,35]. In this technique, the temperature of the combustor walls in the downstream region remains high due to the heat of combustion, and the incoming mixture is preheated by the walls through heat recirculation. Wall thickness and thermal conductivity of solid walls play an important role in the heat recirculation performance of the system configuration. Detailed theoretical analysis and numerical studies on the effect of these parameters on heat recirculation have been reported by Norton and Vlachos [16] and Ronney [17].

To investigate flame stability under microscale conditions, Maruta et al. [21] have studied the flame propagation characteristics of premixed methane–air mixtures in a 2.0-mm-diameter straight quartz tube with a positive temperature gradient in the direction of flow. This is a simple one-dimensional configuration to study flame behavior in microchannels, which resembles a system with heat recirculation through channel walls. A steady state wall temperature gradient was given to the channel walls to simplify the target model. This strategy was employed to avoid thermal coupling between the gas and solid phases, which can be justified if the heat capacity of the solid phase is much greater (thermally thick) than that of the gas phase, which is often true for microchannels. That study showed the existence of a stable premixed flame at high and extremely low mixture velocities. At moderately low velocities, distinct, unstable flame propagation modes such as (a) pulsating flame, (b) flames with repetitive extinction and ignition (FREI) [21], and (c) a combination of pulsating flame and FREI were observed. Linear stability analysis also predicted the existence of different stable and

unstable propagation modes over wide ranges of velocities and equivalence ratios [30].

Motivated by that work, Kumar et al. extended the research to 2-D radial microchannels [31,32]. Experimental observations showed that a variety of flame patterns (see Figs. 1a–1i), such as stable and unstable circular flames, single, double, and triple pelton-like flames, traveling flames, broken flames, triple flames, and spiral flames, existed in those radial microchannels, which were somewhat similar to the configuration of the MIT micro gas turbine [12]. However, Kumar et al. only reported the experimental results at the mixture equivalence ratios of 0.67 and 0.85, and thus current knowledge of flame pattern formations in those radial microchannels is limited. Hence, in order to obtain an overview of the pattern formations and relations between those flame patterns, the present authors conducted systematic experiments at equivalence ratios of 0.65–1.35 and inlet velocity less than 7.0 m/s of a methane–air mixture using an experimental setup identical to that of Kumar et al. [31, 32]. Herein presented are regime diagrams of flame patterns in radial microchannels at channel widths of 0.5, 1.0, 1.5, 2.0, 2.5, and 3.0 mm, as well as combustion characteristics of those flame patterns, which are expected to enrich our knowledge of flame pattern formations in radial microchannels.

2. Experimental setup and methods

A schematic diagram of the experimental setup is shown in Fig. 2. Two circular quartz plates ($\varnothing 50$) were maintained parallel to each other within an accuracy of $\pm 0.1^\circ$. The bottom plate was heated with a sintered metal burner at a constant airflow rate and a constant propane gas flow rate. The top plate was heated by the bottom one via both radiation and convective heat transfer. The typical temperature profiles along the inner surfaces of the bottom and top plates were measured in advance using airflow in the channel of $b = 2.0$ mm and a K-type thermocouple with a 250- μm -sized bead. The head of the thermocouple was bent to keep good contact with the inner surfaces of the two plates. The movement step of the thermo-

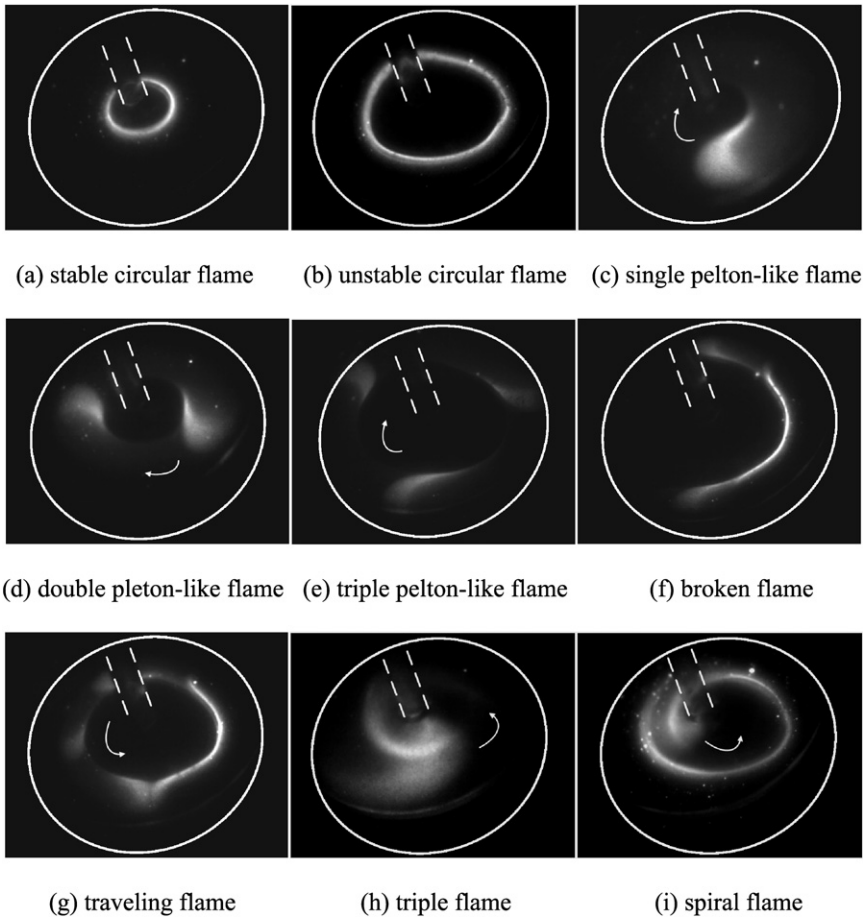


Fig. 1. Photos of various flame patterns observed in radial microchannels: (a) stable circular flame, (b) unstable circular flame, (c) single pelton-like flame, (d) double pelton-like flame, (e) triple pelton-like flame, (f) broken flame, (g) traveling flames, (h) triple flames, and (i) spiral flame. Solid and dashed white lines indicate the position of the top plate and mixture delivery tube, respectively. Arrows are drawn to indicate the rotating direction of the rotating flame patterns.

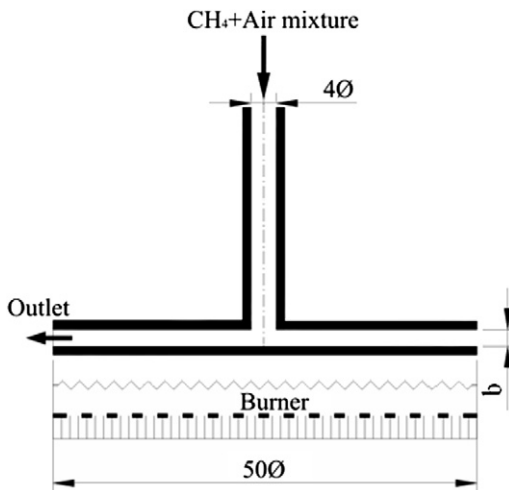


Fig. 2. Schematic diagram of the experimental setup.

couple was 1.0 mm, which was controlled by a transverse micrometer. The measured temperatures were corrected for radiation heat loss from the thermocouple bead and the corrected temperatures are accurate to within ± 5 K of the actual value. Fig. 3 shows the measured temperature profiles when $V_{in} = 4.0$ m/s, from which it can be seen that in most regions the temperature difference between the two plates was less than 30 K. This confirms the validity of the current experimental methodology for forming desired temperature profiles. The mixture delivery tube was designed to maintain the upstream temperature of the incoming mixture at 300 K. The flow rate of the supplied methane–air mixture was monitored through electric mass flow controllers within an accuracy of $\pm 1\%$. To maintain a laminar flow in the delivery tube, the maximum value of the mixture velocity in the delivery tube was set at 7.0 m/s, where the repre-

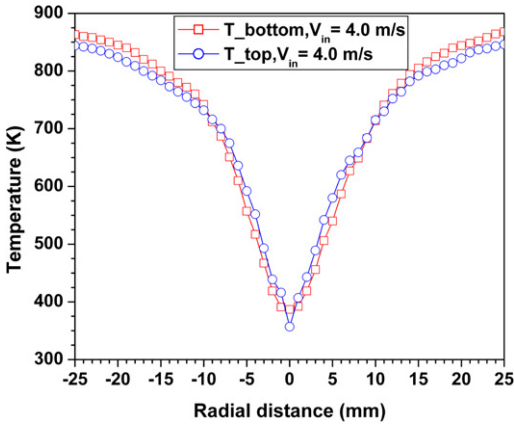


Fig. 3. Measured temperature profiles of the bottom plate and top plate when $V_{in} = 4.0$ m/s and $b = 2.0$ mm.

sentative Reynolds number is about 1800 [31]. The methane–air mixture was ignited by the hot burned gas from the flat flame burner. Images of flames were recorded by a high-speed video camera with an image intensifier at a rate of 500 frames per second with a shutter speed of $1/500$ s. Captured images were analyzed using the software PFV-Ver.2.4.2.0. Exhaust gas analysis was carried out with a Shimadzu GC-14B gas chromatograph. A sample of 500 μ l was drawn with a micro syringe and fed into the gas analyzer. The concentrations of the major species, such as CO_2 , CO , CH_4 , and O_2 , were determined. The uncertainties in the measurements of exhaust gas emissions are less than 3% of the measured values.

3. Regime diagrams and characteristics of flame patterns

Regime diagrams of flame patterns obtained by the present systematic experiments are introduced in Sections 3.1 to 3.6. For each regime diagram, experiments were conducted under all the conditions denoted by the nodes. The nodes without symbols mean that no flame was observed under those conditions. For convenience of discussion, inlet mixture velocity at the delivery tube is used as the horizontal axis instead of the mixture flow rate in those figures.

3.1. Case 1: $b = 0.5$ mm

Fig. 4 shows the regime diagram of flame patterns when the channel width was 0.5 mm. In this figure, only the broken flame pattern (see Fig. 1f) is observed in the inlet mixture velocity range from 3.5 to 6.5 m/s. In this pattern, a certain portion of the flame front remains open. Pelton-like flame fronts originate at the two ends of the semicircular luminous flame

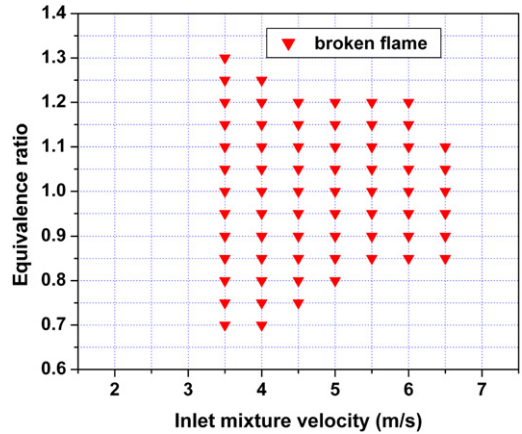


Fig. 4. Regime diagram of flame patterns for the case of $b = 0.5$ mm.

and travel to the central part but do not combine with each other before their disappearance, which leads to an incomplete circular flame. The experimental observations showed that the length and location of the incomplete circular flame front is a function of the equivalence ratio and inlet mixture velocity, although the data are not shown here. Besides, it can also be noted from Fig. 4 that when the inlet mixture velocity is increased, the combustible range of the mixture equivalence ratio becomes narrower.

The imperfect circular configuration of the flame front indicates that a large amount of unburned mixture leaks out of the microchannel.

3.2. Case 2: $b = 1.0$ mm

Fig. 5 is the regime diagram of flame patterns when the channel width was 1.0 mm. The most significant difference between Figs. 4 and 5 is that, besides the broken flame pattern, two other flame patterns, namely, the pelton-like flame (see Fig. 1c) and the traveling flame (see Fig. 1g), appear in Fig. 5. However, only the single pelton-like flame pattern was observed in this case. When the inlet velocity was 2.0 m/s, it is noted that the single pelton-like flame pattern dominates the entire equivalence ratio range of 0.80–1.20. And when the inlet velocity was increased to 2.5 and 3.0 m/s, this pattern only appeared in the regions of $\phi = 0.75$ –0.85 and $\phi = 1.20$ –1.25. No single pelton-like flame pattern was observed at inlet velocities higher than 3.0 m/s. Those single pelton-like flame fronts rotated around the center of the channel in a frequency range of 27.8–55.5 Hz. The traveling flame pattern occupies the central part of regime diagram, which was dominated by the broken flame pattern in Fig. 4. With visual observation, the traveling flame looks like a closed circle with nonuniform luminosities. With further observation with an image

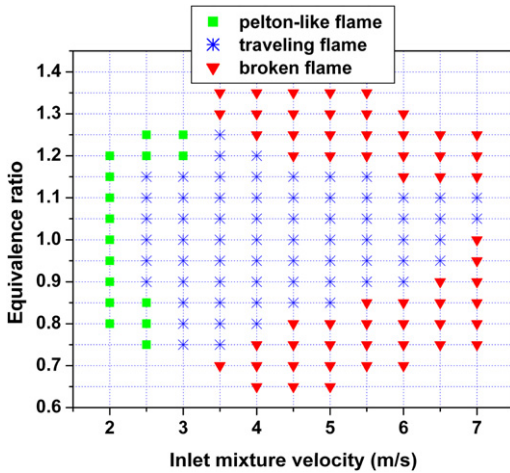


Fig. 5. Regime diagram of flame patterns for the case of $b = 1.0$ mm.

intensified high-speed camera, it can be seen that a flamelet, which is geometrically similar to the pelton-like flame front, emanates from one end of the luminous flame and then travels toward the opposite end. At the moment of its approach, the opposite end of the luminous flame also generates a pelton-like flamelet that merges with the approaching pelton-like flamelet. This character can be clearly seen in Fig. 1g. Another major characteristic of the traveling flame is the relatively loud noise produced by the combustion process. We suppose that it is produced at the moment those two pelton-like flamelets collide with each other in opposite rotation directions, because such noise never appears in the case of the broken flame pattern. In the inlet mixture velocity range from 3.5 to 7.0 m/s, the broken flame pattern occurs in the upper and lower regions of the regime diagram. From an overview of this regime diagram, these three flame patterns are expected to be closely related.

Comparing the lengths of the flame fronts of those three flame patterns, it is obvious that the single pelton-like flame is even worse than the broken flame in terms of combustion efficiency because of a much greater leakage of unburned mixture from the microchannel. Measurements of combustion products showed that the amount of unburned methane of the traveling flame is less than those of the broken and the pelton-like flames, since the traveling flame does not have a wide extinction zone at the flame front. Details of combustion completeness and efficiency of various flame patterns were reported in [34].

3.3. Case 3: $b = 1.5$ mm

The regime diagram of flame patterns when the channel width is 1.5 mm is demonstrated in Fig. 6.

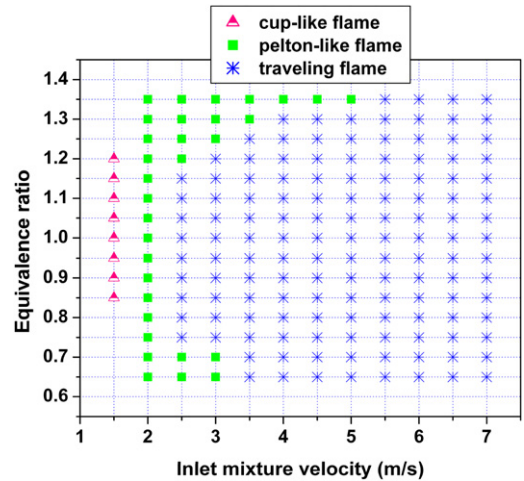


Fig. 6. Regime diagram of flame patterns for the case of $b = 1.5$ mm.

From this figure, it can be seen that the broken flame pattern is no longer observed due to the increase in the channel width and that most of the regime diagram is dominated by the traveling flame pattern. Another phenomenon in the case of $b = 1.5$ mm is the occurrence of multiple pelton-like flames. When $V_{in} = 4.0$ m/s and $\phi = 1.35$, not only a single pelton-like flame (see Fig. 1c) but also a double pelton-like flame (see Fig. 1d) was observed. And under the condition of $V_{in} = 4.5$ m/s and $\phi = 1.35$, besides those two kinds of pelton-like flames, a triple pelton-like flame (see Fig. 1e) also appeared. A further increase in the inlet mixture velocity up to 5.0 m/s resulted in the appearance of tetradic and quinary pelton-like flames, as shown in Figs. 7a and 7b. Tetradic and quinary pelton-like flames are reported here for the first time. On the other hand, multiple pelton-like flames did not appear in fuel-lean mixtures in this case. When the inlet mixture velocity was 1.5 m/s, cup-like flames at the inlet port of the radial microchannel appeared. The cup-like geometry is considered to be a deformed type of conical Bunsen flame and to be caused by the constraint of the narrow channel width.

Fig. 8 shows the rotating frequency variation of the single pelton-like flame front versus the mixture equivalence ratio. From Fig. 8, it can be seen that the maximum value of the rotating frequency appeared at an equivalence ratio of approximately 1.05. This shows that the rotating velocity of the flame front has a positive correlation with the burning velocity of the flame, whose maximum value is attained in a slightly fuel-rich mixture [36]. Furthermore, at the same equivalence ratio, the rotating frequency of the pelton-like flame decreased with an increase in the inlet mixture velocity. The reason for this phenomenon is not very clear at present. One possible explanation

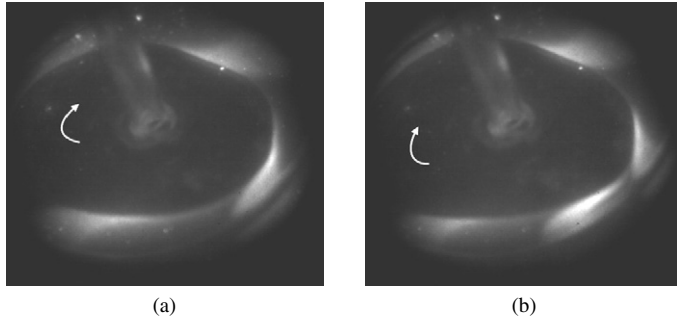


Fig. 7. Photos of tetradic and quinary pelton-like flames under the condition $b = 1.5$ mm, $V_{in} = 5.0$ m/s, and $\phi = 1.35$: (a) tetradic pelton-like flame; (b) quinary pelton-like flame.

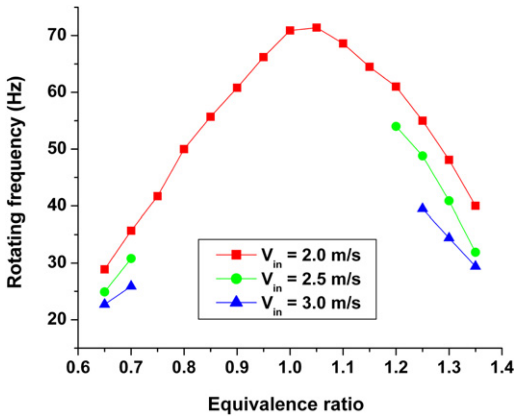


Fig. 8. Rotating frequency of the single pelton-like flame versus equivalence ratio for the case of $b = 1.5$ mm.

is that the radial location of the inner tip of the pelton-like flame front increased with the increase in the inlet mixture velocity, which led to a decrease in the rotating frequency.

3.4. Case 4: $b = 2.0$ mm

Fig. 9 shows the regime diagram of flame patterns when the channel width was 2.0 mm. Comparing Fig. 9 with Figs. 4–6, it can be seen that the central region of the regime diagram is occupied by the stable circular flame pattern (Fig. 1a), which was not seen when the channel width was smaller than 2.0 mm. The flame front of this pattern is a stable, symmetric circle. When the inlet mixture velocity was further increased, the flame front of the circular flame pattern became unstable and was deformed in a viscous liquid deformation manner. At an inlet mixture velocity of 7.0 m/s and in the equivalence range of 0.8–1.0, a rotating flame pattern, i.e., the triple flame (Fig. 1h), was observed. This is thought to be a bifurcation phenomenon in flame fronts. Another distinct feature for the case of $b = 2.0$ mm is that not only in fuel-rich mixtures, but also in fuel-lean mixtures, both single and

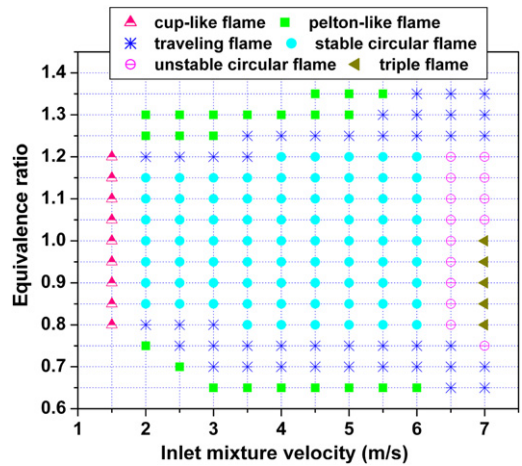


Fig. 9. Regime diagram of flame patterns for the case of $b = 2.0$ mm.

double pelton-like flames were observed. However, the double pelton-like flame only appeared in the inlet mixture velocity ranges of 3.5–5.0 m/s for $\phi = 0.65$ and 4.0–5.5 m/s for $\phi = 1.30$. Other multiple pelton-like flames, which consist of three or more pelton-like rotating flame fronts, have not been observed in the case of $b = 2.0$ mm so far. The region occupied by the traveling flame pattern was significantly decreased and only existed in the circumferences of the stable and unstable circular flame patterns. Finally, cup-like flames also existed when the inlet mixture velocity was 1.5 m/s, as in the case of $b = 1.5$ mm.

The radial location of the stable circular flame is a function of mixture equivalence ratio and inlet mixture velocity, as shown in Figs. 10 and 11. From Fig. 10, it can be seen that under the conditions of $b = 2.0$ mm and $V_{in} = 4.0$ m/s, the variation of flame radius exhibits an inverse tendency with burning velocity. However, the differences between those radii are relatively small. From Fig. 11, on the other hand, it can be seen that for the stoichiometric mixtures, flame radius increased significantly with the increase in the

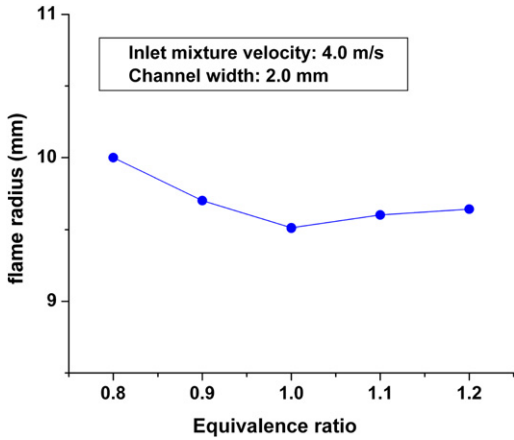


Fig. 10. Radius variation of the stable circular flame versus equivalence ratio under the condition $b = 2.0$ mm and $V_{in} = 4.0$ m/s.

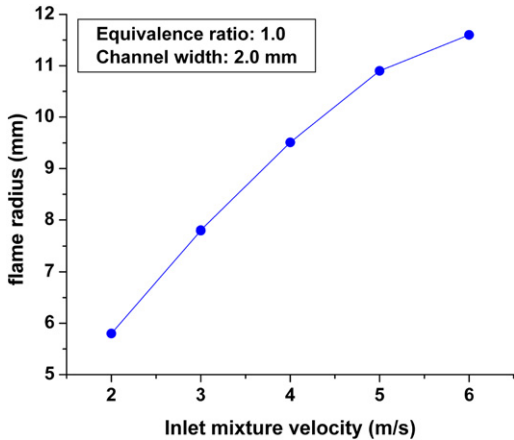


Fig. 11. Radius variation of the stable circular flame versus inlet mixture velocity under the condition $b = 2.0$ mm and $\phi = 1.0$.

inlet mixture velocity. For instance, the flame radius at $V_{in} = 6.0$ m/s was about twice that at $V_{in} = 2.0$ m/s. Those two variation tendencies demonstrate that the radial location of the stable circular flame front is more sensitive to the inlet mixture velocity than to the equivalence ratio.

Fig. 12 presents a comparison between the mole fractions of CO, CO₂, and CH₄ in the exhaust gas flow for single and double pelton-like flames under the condition $\phi = 0.65$ and $b = 2.0$ mm. From Fig. 12, it can be seen that molar fractions of CO₂ and CO for the double pelton-like flame were both higher than those of the single pelton-like flame at the same inlet mixture velocity. Meanwhile, the molar fraction of the unburned fuel, CH₄, of the double pelton-like flame was lower than that of the corresponding single pelton-like flame. Those phenom-

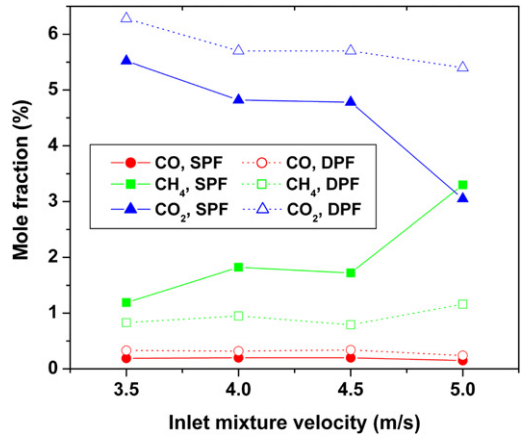


Fig. 12. Mole fractions of CO₂, CO, and CH₄ versus inlet mixture velocity for single and double pelton-like flames under the condition $b = 2.0$ mm and $\phi = 0.65$.

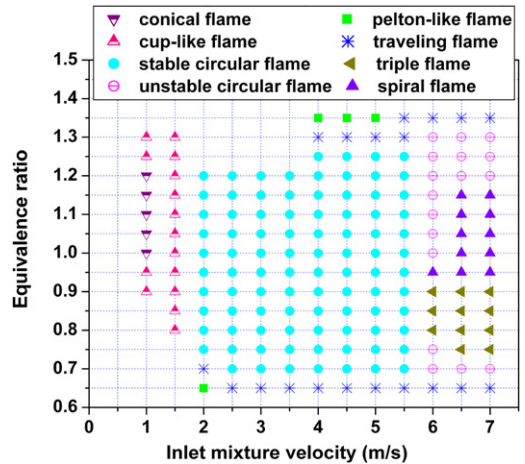


Fig. 13. Regime diagram of flame patterns for the case of $b = 2.5$ mm.

ena are thought to be caused by the differences in flame front numbers between the single pelton-like flame and the double pelton-like flame. For the double pelton-like flame, more fuel is consumed in the combustion process. Those differences were especially obvious when the inlet mixture velocity was increased from 4.5 to 5.0 m/s. When the inlet velocity was 5.0 m/s, the outer radius of the pelton-like flame front almost reached the edges of the circular plates, which led to a high level of unburned mixture leakage.

3.5. Case 5: $b = 2.5$ mm

Fig. 13 shows the regime diagram of flame patterns for the case of $b = 2.5$ mm. Similarly to the case of $b = 2.0$ mm, a stable circular flame pattern dominates the central part of the regime diagram. In the

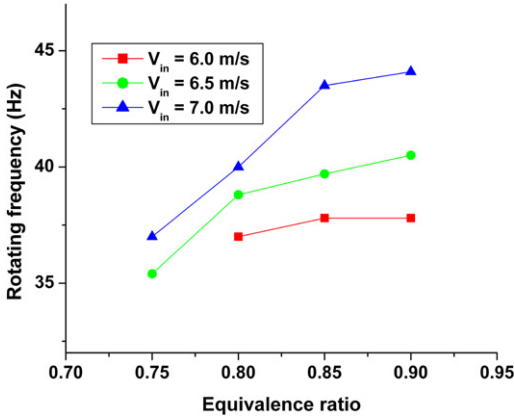


Fig. 14. Rotating frequency of the triple flame versus equivalence ratio in the cases of $b = 2.5$ mm and $V_{in} = 6.0, 6.5,$ and 7.0 m/s, respectively.

high-inlet-velocity region, other than the triple flame pattern, another rotating flame pattern, i.e., the spiral flame (see Fig. 1i), is seen for the case of $b = 2.5$ mm. The spiral-shaped flame front rotates, with its head and tail being much thicker and more luminous than the remaining part. It is also noted from this regime diagram that when the inlet mixture velocity was 1.0 m/s and in the equivalence range of 1.0 – 1.2 , a conical Bunsen flame was observed at the inlet port of the channel. Under conditions of $V_{in} = 1.0$ m/s and $\phi = 0.90, 0.95, 1.25,$ and $1.30,$ and $V_{in} = 1.5$ m/s and $\phi = 0.80$ – $1.30,$ cup-like flames existed at the inlet port of the channel. Regarding the pelton-like flame pattern, only when $V_{in} = 4.5$ and 5.0 m/s and at $\phi = 1.35$ did the double pelton-like flames appear, with the single pelton-like flame existing under other conditions shown in this regime diagram.

Fig. 14 depicts the rotating frequency of the triple flame versus the equivalence ratio at different inlet mixture velocities in the case of $b = 2.5$ mm. From Fig. 14, it can be seen that when the inlet mixture velocity is fixed, the rotating frequency of the triple flame increases with the increase in the equivalence ratio for the fuel-lean mixtures. However, it is noteworthy that the rotating frequency increases with the increase in the inlet mixture velocity at the same equivalence ratio. This variation tendency implies that the rotating frequency of the triple flame has a positive correlation with the inlet mixture velocity, i.e., the flow rate of the fuel–air mixture.

Since the spiral flame front cannot superpose at its original location when it finishes one cycle of rotation, its rotation frequency cannot be accurately calculated. Hence, its variation tendency is not presented here. However, the approximate rotating frequency of the spiral flame is in the range of 38.5 – 41.7 Hz, which smoothly extrapolates to the triple flame rotat-

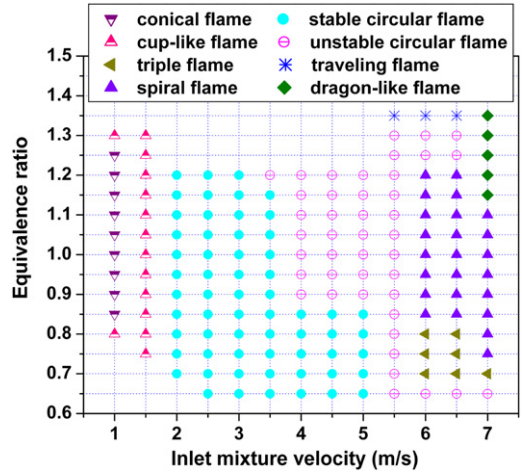


Fig. 15. Regime diagram of flame patterns for the case of $b = 3.0$ mm.

ing frequencies shown in Fig. 14. This implies some similarities in flame pattern formation mechanisms of spiral and triple flames.

3.6. Case 6: $b = 3.0$ mm

Fig. 15 shows the regime diagram of flame patterns when the channel width was 3.0 mm. There are three main features of this figure that are different from those of Fig. 13. First, unstable flame patterns, such as the unstable circular flame, triple flame, and spiral flame, occupy a large part of this regime diagram and the stable flame regime becomes even narrower than that of Fig. 13. Second, a new rotating flame pattern (see Figs. 16a–16i) is observed under conditions of $V_{in} = 7.0$ m/s and $\phi = 1.15$ – 1.35 . Figs. 16a–16i show an entire period of its rotation. From Fig. 16a we can see that the flame front is only a half circle, the head being a little larger than the tail. The head of the flame front then grows larger and becomes more luminous, similarly to the case of the triple flame (see Figs. 16b–16c). Further rotation shows that the number of flame fronts was reduced from 3 to 2 and that the outer part of the flame head grew even larger and became much more luminous (see Figs. 16d and 16e). Meanwhile, the tail of the flame front also became longer (see Figs. 16d and 16e). Further rotation led to the connection of the head and tail of the flame front (see Fig. 16f). At this moment, the geometry of the flame front was somewhat like that of the spiral flame pattern. However, when the flame front continued rotating, it was broken (see Figs. 16g and 16h) and regained its original geometry (see Fig. 16i). Due to the geometrical similarity to a dragon, it is termed the dragon-like flame here. Its rotating frequency is about 35.7 –

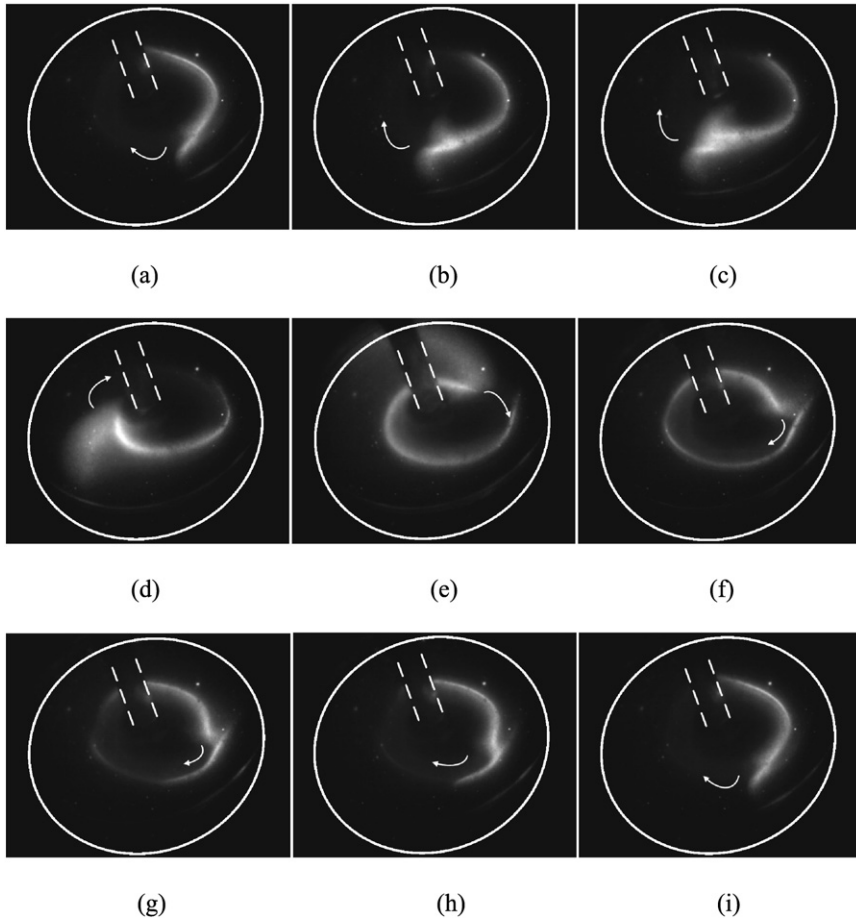


Fig. 16. Sequential photos of a rotation period for the dragon-like flame pattern under the condition of $b = 3.0$ mm, $V_{in} = 7.0$ m/s, and $\phi = 1.15$.

38.5 Hz. From the whole evolution process of the flame front, we suppose that the dragon-like flame pattern combines the triple and spiral flame patterns. From Fig. 15, it can be seen that the triple flame pattern and the dragon-like flame pattern exist in the lower and upper regions of the spiral flame pattern, respectively, which also implies that those three flame patterns may be closely related. The third main feature of Fig. 15 is the disappearance of the pelton-like flame pattern from this regime diagram. Even in very rich and lean mixtures, it was no longer observed.

4. Discussion

In the preceding section, it has been shown that combustion in a radial microchannel is much more complex than that in a straight tube [21] because of the additional freedom in the angular direction. The effects of positive temperature gradient and negative

velocity gradient in the direction of flow can lead to the formation of various rotating flame patterns.

In the context of microscale combustion, Minaev et al., introduced an evolutionary 1-D equation for the flame front, which was investigated by the bifurcation theory and numerical simulations [30]. This model was able to explain the different phenomena including the flame ignition, the flame extinction, and the flame oscillations observed in the straight microscale tube [21]. In the paper [33], the 2-D evolutionary equation for the flame front in the channel with temperature gradient had been proposed to describe the traveling waves propagating along the flame front. The spiral structure was considered as a solitary wave propagating with constant velocity along the flame. Being projected into the cylindrical case, this solution could take the form of a spiral rotating with constant angular velocity around the axis of symmetry. However, this study [33] also showed that formation mechanisms responsible for other unstable flame patterns, such as the triple flame pattern, cannot be explained

in the same way. This indicates that pattern formation mechanisms of those flame patterns may be different. Comparing Fig. 8 with Fig. 14, it can be seen that the pelton-like flame and the triple flame exhibit opposite variation tendencies of the rotating frequency with respect to inlet mixture velocity. These facts suggest that hydrodynamic instability or joint action of hydrodynamic and thermodiffusion effects [37–41] in the presence of a channel temperature gradient are responsible for the formation of some rotating patterns.

Although detailed mechanisms of formation of those rotating structures still remain unclear, the present experimental study produced regime diagrams of existence of different flame patterns. For instance, the broken flame was the sole flame pattern observed in the case of $b = 0.5$ mm, and it also appeared in the case of $b = 1.0$ mm. However, it disappeared when the channel width was increased to 1.5 mm. The pelton-like flame pattern existed either under low inlet mixture velocity or in cases of low and high equivalence ratios. The occurrence of multiple pelton-like flames depended strongly on equivalence ratio, inlet mixture velocity, and channel width. Stable circular flames were not observed until the channel width was increased to 2.0 mm and they occupy a large area of the regime diagram when $b = 2.0$ mm. However, with a further increase in the channel width, the stable flame region became narrower and regions occupied by unstable flame patterns, such as unstable circular flame, triple flame, spiral flame, and dragon-like flame, became larger. This demonstrates that an increase in channel width does not mean that a wider stable combustion region could be obtained, which provides us useful information for the design and practical operation of such kinds of microcombustors.

Furthermore, the regime diagrams presented in Section 3 distinctly show that the existence of all those flame patterns was a strong function of the inlet mixture velocity, equivalence ratio, and channel width. Those regime diagrams also demonstrate the relations between the various flame patterns. Our experimental findings show that a small variation in one of the three parameters, i.e., inlet mixture velocity, equivalence ratio, and channel width, can result in flame pattern transitions. For instance, pelton-like flames can transit to traveling flames, and unstable circular flames can transit to spiral flames and triple flames, and so forth, by a small variation in equivalence ratio or inlet velocity. Those results will be reported in our next paper.

5. Summary

By varying the mixture equivalence ratio, inlet mixture velocity, and channel width, flame pattern

formations in radial microchannels with a temperature gradient were comprehensively investigated and regime diagrams at channel widths of 0.5, 1.0, 1.5, 2.0, 2.5, and 3.0 mm were presented in this paper. A clear overview of the distributions of all the flame patterns was obtained from the present regime diagrams. Some combustion characteristics of each flame pattern, such as rotating frequency, concentrations of major combustion products, and radius of flame front, were also presented and discussed. Knowledge of those characteristics enables better understanding of the various stable and unstable flame patterns, which can contribute to future clarification of flame pattern formation mechanisms. Findings of the present study should also contribute to improvements in the practical design and operation of radial microscale combustors with heat recirculation.

Acknowledgment

The authors thank S. Hasegawa for helping to conduct the present experiments.

References

- [1] M. Gorman, M. el-Hamdi, B. Pearson, *Phys. Rev. Lett.* 76 (1996) 228–231.
- [2] A. Bayliss, B.J. Matkowsky, *Physica D* 99 (1996) 276–302.
- [3] H.G. Pearlman, P.D. Ronney, *Phys. Fluids* 6 (1994) 4009–4018.
- [4] V. Panfilov, A. Bayliss, B.J. Matkowsky, *Appl. Math. Lett.* 16 (2003) 131–135.
- [5] V. Nayagam, F.A. Williams, *Phys. Rev. Lett.* 84 (2000) 479–482.
- [6] H.G. Pearlman, *Combust. Flame* 109 (1997) 382–398.
- [7] G.R. Ruetsch, L. Verisch, A. Linan, *Phys. Fluids* 7 (6) (1995) 1447–1454.
- [8] G.I. Sivashinsky, *Annu. Rev. Fluid Mech.* 15 (1983) 179–199.
- [9] F.A. Williams, *Combustion Theory*, Benjamin-Cummings, 1985, p. 341.
- [10] O. Zik, Z. Olami, E. Moses, *Phys. Rev. Lett.* 81 (1998) 3868–3871.
- [11] M.L. Frankel, G.I. Sivashinsky, *Phys. Rev. E* 52 (1995) 6154–6158.
- [12] A.H. Epstein, S.D. Senturia, G. Anthasuresh, in: *IEEE Transducers '97 Conf.*, Chicago, IL, 1997, pp. 753–756.
- [13] A. Mehra, X. Zhang, A.A. Ayon, I.A. Waitz, M.A. Schmidt, C.M. Spadaccini, *J. Microelectromech. Syst.* 9 (2000) 517–527.
- [14] J. Vican, B.F. Gajdeczko, F.L. Dryer, F.L. Milius, A. Aksay, R.A. Yetter, *Proc. Combust. Inst.* 29 (2002) 909–916.
- [15] A.C. Fernandez-Pello, *Proc. Combust. Inst.* 29 (2002) 883–890.

- [16] D.G. Norton, D.G. Vlachos, *Chem. Eng. Sci.* 58 (2003) 4871–4882.
- [17] P.D. Ronney, *Combust. Flame* 135 (2003) 421–439.
- [18] C.M. Spadaccini, A. Mehra, J. Lee, X. Zhang, S. Lukachko, I. Waitz, *J. Eng. Gas Turbines Power* 125 (2003) 709–719.
- [19] A.V. Pattekar, M.V. Kothare, *J. Microelectromech. Syst.* 13 (2004) 7–18.
- [20] N.I. Kim, S. Kato, T. Kataoka, T. Yokomori, S. Maruyama, T. Fujimori, K. Maruta, *Combust. Flame* 141 (2005) 229–240.
- [21] K. Maruta, T. Kataoka, N.I. Kim, S. Minaev, R. Fursenko, *Proc. Combust. Inst.* 30 (2005) 2429–2436.
- [22] K. Maruta, J.K. Parc, K.C. Oh, T. Fujimori, S.S. Minaev, R.V. Fursenko, *Combust. Explos. Shock Waves* 40 (2004) 516–523.
- [23] J. Hua, M. Wu, K. Kumar, *Chem. Eng. Sci.* 60 (2005) 3507–3515.
- [24] M. Wu, J. Hua, K. Kumar, *J. Micromech. Microeng.* 15 (2005) 1817–1823.
- [25] C. Miesse, R. Masel, M. Short, M. Shannon, *Combust. Theory Modeling* 9 (2005) 77–92.
- [26] S. Prakash, A.D. Armijo, R.I. Masel, M.A. Shannon, *AIChE J.* 53 (2007) 1568–1577.
- [27] F. Richecoeur, D.C. Kyritsis, *Proc. Combust. Inst.* 30 (2005) 2419–2427.
- [28] T.T. Leach, C.P. Cadou, *Proc. Combust. Inst.* 30 (2005) 2437–2444.
- [29] T.S. Cheng, Y.C. Chao, C.Y. Wu, Y.H. Li, Y. Nakamura, K.Y. Lee, T. Yuan, T.S. Leu, *Proc. Combust. Inst.* 30 (2005) 2489–2497.
- [30] S. Minaev, K. Maruta, R. Fursenko, *Combust. Theory Modeling* 11 (2007) 187–203.
- [31] S. Kumar, K. Maruta, S. Minaev, *Phys. Rev. E* 75 (2007) 016208.
- [32] S. Kumar, K. Maruta, S. Minaev, *Proc. Combust. Inst.* 31 (2007) 3261–3268.
- [33] S. Minaev, S. Kumar, K. Maruta, in: *Proc. ASPACC*, 2007, pp. 546–549.
- [34] A.W. Fan, S. Minaev, S. Kumar, W. Liu, K. Maruta, *J. Micromech. Microeng.* 17 (2007) 2398–2406.
- [35] S.A. Lloyd, F.J. Weinberg, *Nature* 251 (1974) 47–50.
- [36] S.R. Turns, *An Introduction to Combustion*, second ed., McGraw–Hill, New York, 2000, pp. 278–279.
- [37] G.I. Barenblatt, Y.B. Zeldovich, A.G. Istratov, *J. Appl. Mech. Tech. Phys.* 4 (1962) 21–26.
- [38] G.I. Sivashinsky, *Acta Astronaut.* 4 (1977) 1177–1206.
- [39] G. Joulin, P. Clavin, *Combust. Flame* 35 (1979) 139–153.
- [40] L. Landau, *Acta Physicochim. URSS* 19 (1944) 77–85.
- [41] J. Yuan, Y. Ju, C.K. Law, *Phys. Fluids* 17 (2005) 074106.